Time structure of chaotic attractors: A graphical view

P. Maurer,[1] Hai-Da Wang,[1] and A. Babloyantz[2]
[1]*International Solvay Institutes, Code Postale 231, Boulevard du Triomphe, Bruxelles, Belgium*
[2]*Center for Non-linear Phenomena and Complex Systems, Code Postale 231, Boulevard du Triomphe, Bruxelles, Belgium*
(Received 4 February 1997)

We present a simple and computationally inexpensive graphical method that unveils subtle correlations between short sequences of a chaotic time series. Similar events, even from noisy and nonstationary data, are clustered together and appear as well-defined patterns on a two-dimensional diagram and can be quantified. The general method is applied to the electrocardiogram of a patient with a malfunctioning pacemaker, the residence times of trajectories in the Lorenz attractor as well as the logistic map. In each case the diagrams unveil different aspects of the system's dynamics. [S1063-651X(97)06607-5]

PACS number(s): 07.05.Rm, 05.45.+b, 87.90.+y, 02.30.Lt

I. INTRODUCTION

The characterization of chaotic attractors from a time series analysis in general requires long, noiseless, and stationary data sets, which are not always available [1–6]. On the other hand, the existing algorithms, such as the dimension estimation or the evaluation of Lyapunov exponents or entropies, are prone to some degree of error [7–17]. In general, with these methods it is difficult to distinguish between two chaotic dynamics that have similar invariants of motion. In addition, these methods are computationally expensive and time consuming. Moreover, whenever the differential equations describing the chaotic attractors are available, it may happen that a very small change in one of the parameters will change completely the nature of the chaotic attractor. It may not always be possible to detect these changes by the usual methods. In this paper we show that a graphical method with similarity to the technique of the first-return maps [18–20], correlating three, four, five, etc., events, can be very informative in reveling subtle differences between two different time series. The method is extremely simple and computationally economical [21,22]. The correlations are displayed in two-dimensional ''*variability diagrams*'' for easy visual inspection. In the presence of deterministic chaos, well-defined structures are seen. These structures are a fast and convenient visual tool for unveiling some detailed aspects of system dynamics. It also enables quantification of regular sequences of data of various lengths and the clustering of similar events.

We shall illustrate the method by studying three attractors. In the first example, a time series is obtained by measuring the time interval between two successive heartbeats denoted as RR of a patient with an implemented malfunctioning pacemaker. We show how in this case useful and detailed quantitative information could be obtained from various diagrams, which are not available with other standard techniques of medical literature such as the fast Fourier transform and the standard deviation of the distribution function as well as from the phase-space construction and first-return maps [23–26].

In the second example we consider a time series composed of the successive residence times t_i of the trajectories of the Lorenz attractor in the basin of attraction of the two fixed points across the plane $x=0$. We also consider the succession of times T_i when trajectories cross the plane only in one direction. T_i represent the unstable periods of the system. It is shown that in both cases well-defined relationships between the successive residence times and successive periods T_i exist. Moreover, in the first case, the structure of the first-order variability diagrams could be related to the number of rotations of trajectories around a given point. It is also shown that the acceleration and deceleration of dynamical events follow different rules.

In the third example we examine the logistic map, considered in the chaotic regime. Here we also show that a small change of the bifurcation parameter introduces a new sequence of events, indicating a qualitative change in the nature of the attractor, which can be seen immediately with the help of the graphical method.

II. VARIABILITY DIAGRAMS

We consider a time series representing discrete temporal events, discrete variables, or measurements in succession, denoted by r_i. This time series may result either from an unknown dynamical system or as a solution to a set of differential equations or chaotic maps. Higher-order forward differences for a set of equally spaced discrete variables of a function r at a point i are defined as [27]

$$\Delta_i^n=\sum_{k=0}^{n}(-1)^k\binom{n}{k}r_{i+n-k},\quad i,n=1,2,3,\ldots\ .$$

From m consecutive points, we construct an m-dimensional vector in the following manner:

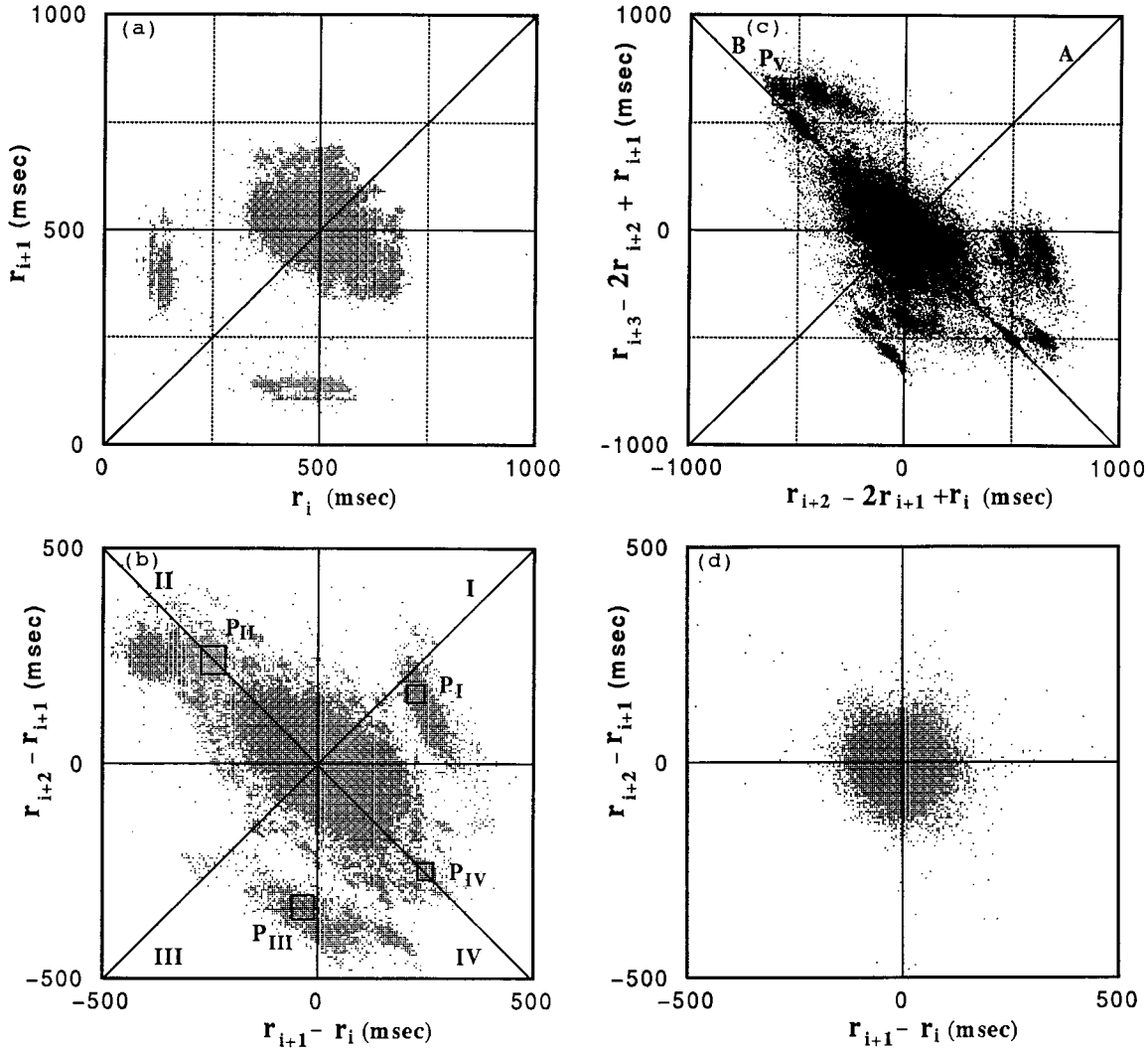

FIG. 1. (a) First-return map constructed from time intervals between two heart beats (RR). The 24-h recording was obtained from a Holter device. (b) First-order variability diagram. (c) Second-order variability diagram. (d) First-order diagram of RR intervals from the 24-h Holter recording of a normal individual.

$$X_i^{(n)}=\sum_{k=0}^{n}(-1)^k\binom{n}{k}r_{i+n-k},$$

$$X_{i+1}^{(n)}=\sum_{k=0}^{n}(-1)^k\binom{n}{k}r_{i+n+1-k},\quad n=0,1,2,\ldots \qquad (1)$$

$$\vdots$$

$$X_{i+m-1}^{(n)}=\sum_{k=0}^{n}(-1)^k\binom{n}{k}r_{i+n+m-1-k},$$

which projects the evolution of the system's dynamics into an m-dimensional space. n is the number of consecutive elements in a time series. In the presence of chaotic dynamics well-defined structures for all n could be seen.

For the particular case $n=0$ and $m=2$, one recovers the familiar first-return map, which is denoted as the zeroth-order ''variability diagram'' and correlates two adjacent points [see Fig. 1(a)].

If $n=1$ and $m=2$, then $X_i^{(1)}=r_{i+1}-r_i$ and $X_{i+1}^{(1)}=r_{i+2}-r_{i+1}$ and we speak of a *first-order* variability diagram in two dimensions. This diagram correlates three successive values. By nature of its construction, if three magnitudes are identical, then $X_i^{(1)}=X_{i+1}^{(1)}=0$. Any positive or negative value of coordinates indicates a departure from absolute periodicity in the values of r. If $X_i^{(1)}>0$ and $X_{i+1}^{(1)}>0$, then we are in the presence of three successive intervals such that, at each step the value of r increases. If r represents time intervals, this shows a kind of deceleration in the dynamical process. The corresponding point will populate quadrant I [see Fig. 1(b)]. On the contrary, $X_i^{(1)}<0$ and $X_{i+1}^{(1)}<0$ indicate a gradual shortening of the values of r, thus an acceleration of the process. The corresponding point appears in quadrant III. Short-long-short values of r are represented by $X_i^{(1)}>0$ and $X_{i+1}^{(1)}<0$, whereas $X_i^{(1)}<0$ and $X_{i+1}^{(1)}>0$ are related to long-short-long values. They populate, respectively, quadrants II and IV. Let us note that the first-order variability diagram is a very different projection from the first-return map constructed in three-dimensional space, which also correlates these quantities [28].

A *second-order* variability diagram can be constructed by taking $n=2$ and $m=2$; then $X_i^{(2)}=r_{i+2}-2r_{i+1}+r_i$ and $X_{i+1}^{(2)}=r_{i+3}-2r_{i+2}+r_{i+1}$. Figure 1(c) shows such a diagram. The points on the diagonal A obey the relation $r_i-3r_{i+1}+3r_{i+2}-r_{i+3}=0$, whereas the diagonal B is the locus of points such as $r_{i+1}-r_i=r_{i+3}-r_{i+2}$.

Once a pattern is seen in a low-order diagram, the numerical value of the r_i forming the pattern can be found easily. For example, in the case of a first-order diagram, we choose a pattern or a piece of pattern of interest and isolate the corresponding points. We construct a first-return map from these points only, which will reveal their numerical values if combined with information obtained from the first-order diagram. If, for example, the pattern emerges from quadrant I ($X_i^{(1)}>0$ and $X_{i+1}^{(1)}>0$), following the definition of Eqs. (1), we have the extra information $r_{i+2}>r_{i+1}>r_i$ needed in combination with first-return maps to determine the exact values of successive threesomes. This procedure will become more clear in the next section. Similar reasoning is used for a second-order diagram in two dimensions. Again, this will be illustrated in the following section.

As the order of diagrams increases, the interpretation of patterns in two-dimensional space becomes difficult; nevertheless, they still are very useful for a visual inspection of system dynamics. However, as the origin of coordinates is also the locus of $n+2$ successive and equal values in an $m=2$ space, Eqs. (1) are a means of sorting out, displaying in a cluster, and also quantifying all these almost equal stretches whenever they arise in a long data set.

Let us note that the first-order variability diagram can be considered as the mapping of the forward differences of the function at two successive points, whereas the second-order diagram is the mapping of second-order differences taken at two adjacent points. As the order of the diagrams increases, the domain of correlations increases also. Inspired by this idea, we introduced the method of variability diagrams, which should not be confused with multidimensional first-return maps.

III. CARDIAC ATTRACTOR

A patient with a cardiac pathology received a pacemaker implant, which unfortunately did not function properly. The electrocardiogram of this patient was recorded over 24 h with a Holter device and the time interval between two successive beats, so-called RR intervals, were evaluated with commercial software. Even if the heart of a patient were normal, a degree of variability would still be seen. Figure 1(d) depicts the first-order variability diagram of a normal individual. It is seen that the difference between two successive RR intervals does not exceed 200 msec. However, in the case of our patient the pacemaker did not fulfill its role properly and could not restore normal dynamics of the cardiac activity. There is a competition between the ailing heart and the pacemaker. This gives rise to an extremely large heart rate variability (HRV). The analysis of the temporal structures and the numerical values of the sequences of events in this particular heart may furnish valuable clues to the cardiologist.

Figure 1(a) shows the first-return map of this patient. The HRV is separated into three parts. All we can say from this diagram is that the two small patches represent, respectively, RR intervals of 320–500 msec followed by short intervals of 100–150msec and the same short interval followed by large intervals ranging between 350 and 575 msec. The content of the third patch is still less informative as it merely describes RR intervals in the range 375–700 msec that follow each other.

In our variability diagrams the number of patches increases as the order of diagrams increases. Therefore, the resolution of the sequence analysis increases substantially. Moreover, the successive values of longer pieces of data become available. Figures 1(b) and 1(c) exhibit, respectively, the first- and second-order variability diagrams. In a diagram of nth order, each point has a coordinate defined by

$$X_i^{(n)}=\sum_{k=0}^{n}(-1)^k\binom{n}{k}r_{i+n-k},$$
$$X_{i+1}^{(n)}=\sum_{k=0}^{n}(-1)^k\binom{n}{k}r_{i+n+1-k}. \tag{2}$$

Let us analyze in detail some subparts of the first-order diagram. According to the definition of Eqs. (2), quadrant I corresponds to a deceleration of the heart over three RR intervals. For example, we consider the patch denoted by P_{I} in Fig. 1(b) and construct the first-return map only from these points. From the discussion Sec. II, it is easy to find that three successive RR intervals in the neighborhood of 145, 375, and 535 msec [see Fig. 2(a)] contribute to the HRV. Similarly, the analysis of P_{III} in quadrant III shows contributions in the neighborhood of the sequences 500, 470, and 140 msec. Figure 2(b) is the first-return map constructed from the selected points in patch P_{II} in quadrant II. Therefore, we can deduce that two different sequences (380, 140, and 380 msec and 620, 380, and 620 msec) contribute to patch P_{II}. In the same fashion a piece for quadrant IV (P_{IV}) shows the following events: 130, 380, and 130 msec and 400, 650 and 400 msec. This illustrates the fact that the diagrams cluster together sequences of events that conserve a given relationship. Referring to the definition of the first-order diagram, the points contained in a square of half-width of 50 msec centered around the origin give an estimation of the regularity of the heart or sinus rhythm over three beats [23]. This choice allows only a difference of 50 msec between two successive RR intervals. In our example, if a first-return map is constructed from these points, the regularity only appears in the range 450–550 msec and includes 32.47% of the total data, indicating the degree of efficiency of the pacemaker. This contrasts with the value of 75.36% found in the normal heart of Fig. 1(d). Similar quantitative discussions could be made for all patches or any chosen areas of the large central patch.

Now let us analyze the second-order variability diagram of Fig. 1(c). Again every patch could be analyzed separately by keeping in mind that we are in the presence of four RR intervals, denoted as r_i, which obey

$$X_i^{(2)}=r_{i+2}-2r_{i+1}+r_i,$$
$$X_{i+1}^{(2)}=r_{i+3}-2r_{i+2}+r_{i+1}. \tag{3}$$

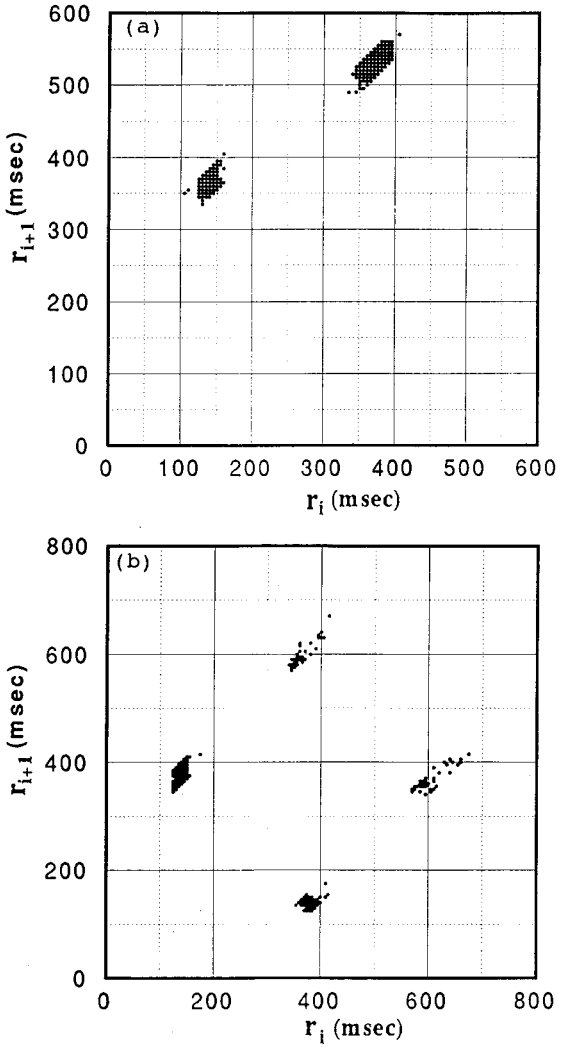

FIG. 2. (a) First-return map of selected points from the pattern in the square P_{I} in Fig. 1(b). (b) First-return map of selected points from a square at P_{II} in Fig. 1(b).

The RR values obtained from the first-return map together with the sign and numerical values of $X_i^{(2)}$ and $X_{i+1}^{(2)}$ for a given patch makes it possible, for example, to conclude that the structure P_{V} in quadrant II has contributions from the vicinity of the four successions of 270, 530, 140, and 530 msec. The number of points in the square of the half-width of 50 msec centered around the origin accounts for 23.63% of that of the total data. Let us note that this number encompasses not only a sinus rhythm but also all foursomes obeying Eqs. (3). The same analysis can be performed for any selected area in the second-order variability diagram with the help of the graphical method presented in this paper.

Let us note that all points on the diagonal B of the second-order diagram have a particular relationship as $X_{i+1}^{(2)} = -X_i^{(2)}$ and they correspond to an alternation in the four consecutive RR intervals.

The analysis of higher-order diagrams is not easy. However, they can still be useful in two ways. A visual inspection of the diagrams may furnish information about the time series. Although it is not easy to estimate the values of $n+2$ successive events for all patches, the fact that a patch exists indicates the existence of privileged relationships between

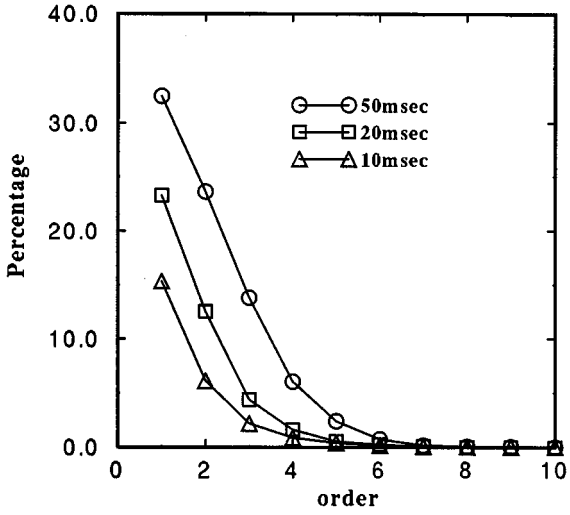

FIG. 3. Percentage of $n+2$ regular sequences as a function of the order of diagrams constructed from RR intervals of the patient in Fig. 1.

the events obeying the definition of Eqs. (2); thus they follow a sort of regular behavior. Moreover, the points around the origin of diagrams of all order stem from complex relationships between RR intervals. However, very close to the origin, the most probable combination is a sequence of almost equal RR intervals. Figure 3 shows the percentages of these sequences contained in a square centered at the origin of a half-width of 25, 10, and 5 msec, respectively, for variability diagrams up to order 10. These values must be compared with the 5-msec error measurements of RR values.

We see that with the help of variability diagrams it is possible to analyze in detail short stretches of cardiac events over 24-h periods, find the regularities, and evaluate sequence values. The fact that these results are displayed on a two-dimensional diagram and require an extremely simple and fast algorithm makes it of great value for medical diagnoses.

IV. LORENZ ATTRACTOR

In this section we use the variability diagrams to unveil some aspects of temporal structures that arise in the well-known Lorenz attractor. The Lorenz attractor is described by the set of dimensionless differential equations

$$\frac{dx}{dt} = P_r(y-x),$$

$$\frac{dy}{dt} = -xz + rx - y,$$

$$\frac{dz}{dt} = xy - bz, \tag{4}$$

with $P_r = 10$, $b = 2.66$, and $r = 28$. With this set of parameters the dynamics described by Eqs. (4) exhibits chaotic behavior. The trajectories of the system evolve around two fixed points with random residence times.

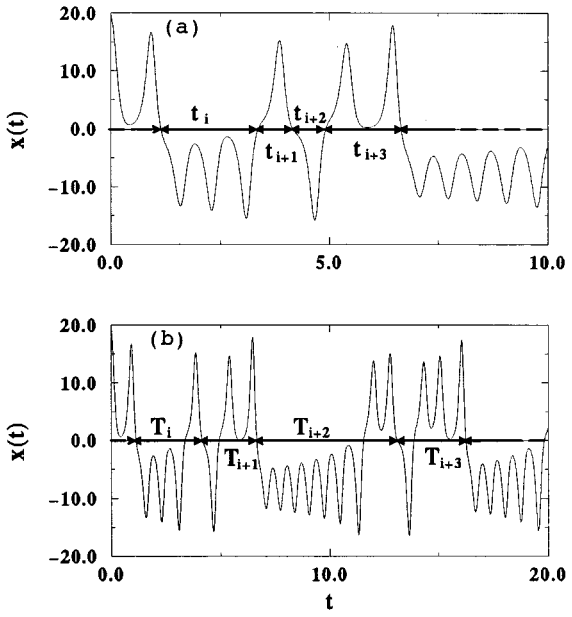

FIG. 4. Temporal evolution of variable $\mathbf{x}(t)$ of the Lorenz attractor. (a) Definition of t_i. (b) Definition of T_i. All variables and parameters are dimensionless.

Two series of events will be considered. In the first case we record the residence time t_i around each fixed point [29]. Figure 4(a) shows the time of passage across the $x=0$ plane. In the second case $T_i=t_i+t_{i+1}$ is the sum of the two successive residence times around each fixed point or the period of an unstable orbit [Fig. 4(b)].

Figure 5(a) shows the general structure of the first-order variability diagram constructed from the time series t_i. One sees immediately well-defined and quantized structures in the case of Lorenz attractor, whereas a random noise will show a homogenous distribution of intervals [21]. The details of the structure as well as its general shape result from the distribution function of t_i, which is not uniform and exhibits several discrete peaks. This fact explains the blurred boundaries of the diagram and also the form of the structure in the second quadrant.

In the first-order variability diagram, all four quadrants exhibit different densities of the population of points. Figure 5(b) is a magnification of the events in the vicinity of the origin of the axis. One sees immediately several well-defined curves, which suggest well-defined temporal sequences. However, the most salient feature is the assymmetry between the four quadrants. From the definition of the first-order diagram we infer that three successive shortening, three successive increasing, and long-short-long and short-long-short times are not related in the same manner. A detailed inspection of other substructures shows again that in each quadrant a different structure is seen.

The first-order variability diagram can furnish detailed information about the physiognomy of the attractor. The checkerboard-type structure is specific to the Lorenz attractor. Each element of the checkerboard is a grouping of all t_i with a well-defined relationship regardless of the intrinsic magnitude. The U-shaped patterns are predominant in the upper half plane. They indicate that two t_i of comparable magnitude are followed by a much larger t_i. On the contrary, in the lower half plane they indicate two large t_i followed by a much smaller time.

From the first-order variability diagram we can deduce the pattern of rotation of trajectories around the two fixed points in the course of three transitions across the $x=0$ plane. We consider the number of rotations made by the trajectories around one of the fixed points before the transition to the basin of attraction of the second fixed point and measure the time. Figure 6 shows this number as a function of time. As expected, for a given number of rotations, a large time variation is seen. If one neglects regions of small overlaps with small probability, it is possible to correlate residence times with the number of turns around one of the fixed points. In overlapping regions an error of one turn is possible.

Let us consider the cluster of points around the origin in the square of size $[(-0.3,-0.3),(0.3,0.3)]$. It accounts for 17.737% of data set and by construction indicates three almost equal t_i in succession. A first-return map constructed only from these points [see Fig. 5(d)] gives the t_i for each threesome. With the help of Fig. 6 we see that one to six consecutive and equal turns are possible in this data set.

A similar analysis indicates that the first structures *a* on the diagonal in quadrant I [see Fig. 5(b)] group a succession of residence times such that in each step one more turn is added to the trajectories (1.496%). The lowest combination is one turn followed by two and three turns. The reverse situation is seen for the first structures *b* on the diagonal of quadrant III (1.502%). Here a high number of rotations decreases by a unit in each transition. The lowest combination is 3, 2, and 1.

In substructures *c* two n turns are followed by an $n+1$ turn, with a minimum of $n=2$ (0.733%). In *d* the succession is n, $n+1$, and n with $n_{\min}=1$ (5.859%). Structures further away from the center indicate a larger variation in the number of successive turns. For example, if we consider only the various L-shaped curves on the diagonal of quadrant IV the following combination [25] are seen starting from substructure *d*: 1, 2, and 1 and 1, 3, and 1 (2.854%); 1, 4, and 1 (1.6345%), etc. In *e* of quadrant II we have $n+1$, n, and $n+1$ with 0.4% of the data set.

Such a detailed analysis of the temporal picture of the attractor can be performed for all substructures or any small piece of a substructure of Fig. 5(a). The following picture emerges from this analysis. For the data set considered, all combinations of the numbers of rotations are possible. However, the most probable one is three successive transitions of the same number of turns. The next most probable combination is 1, n, and 1, with $n=2-4$.

Figure 5(c) shows the details in the vicinity of the origin of the second-order variability diagram. One still sees well-defined patterns and dissymmetry of curves in the four quadrants. Keeping the integration time constant, we constructed diagrams up to eight order. At this order one still sees structured patterns, although somewhat blurred. This may be due in part to the fact that as the order of diagrams increases the coordinates of points also increases [see definitions (2)] and there are few points for defining a curve. An analysis similar to the one performed above is still possible for second-order variability diagrams and will not be reported here.

Second-order variability diagrams from t_i are convenient visual aides for finding the first-order periods of the Lorenz

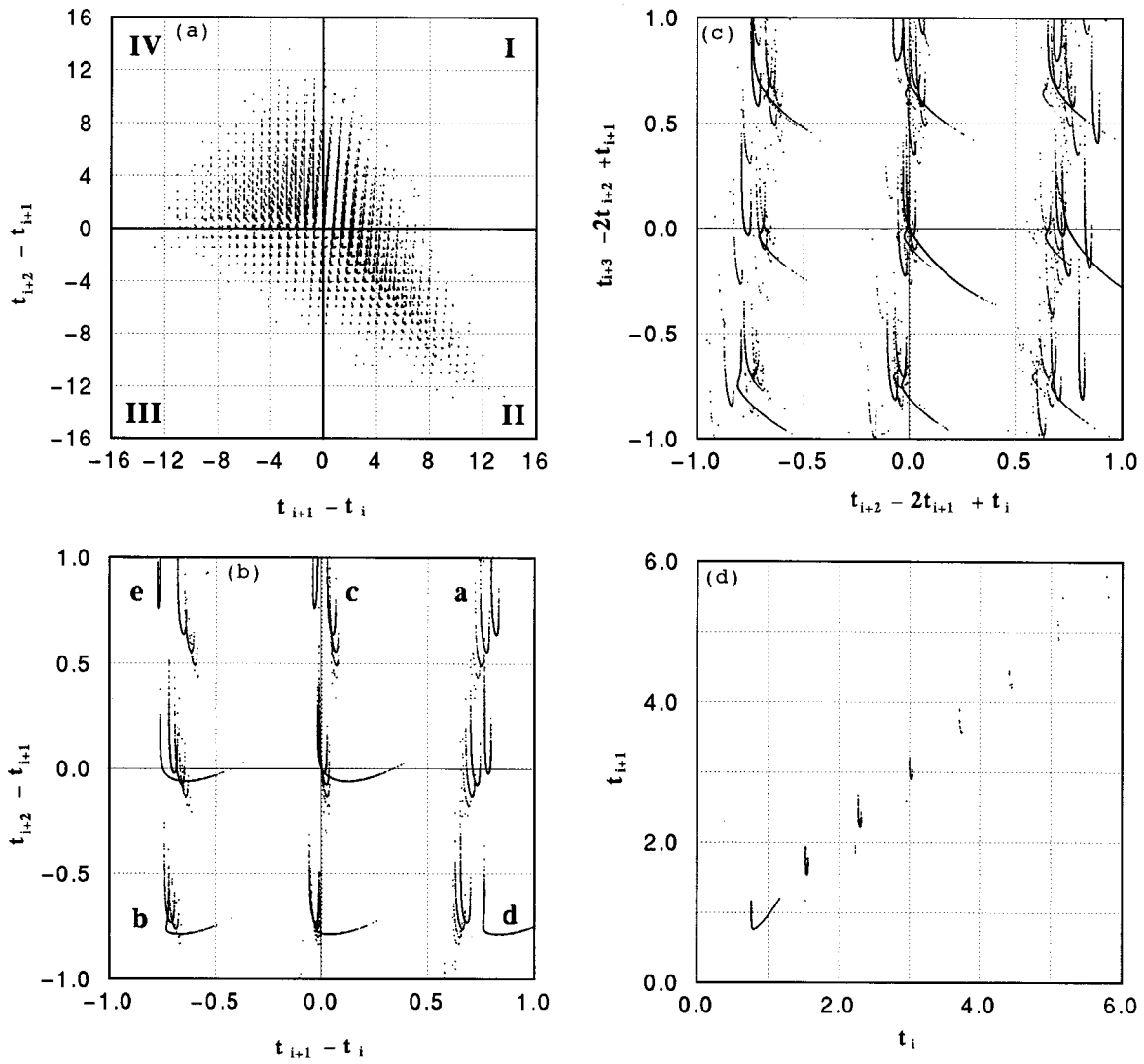

FIG. 5. (a) First-order variability diagram of the Lorenz attractor for t_i. (b) Magnification of the diagram in the vicinity of the origin. (c) Magnification of a second-order variability diagram. (d) First-return map constructed from the points around the original in (b). All variables and parameters are dimensionless.

attractor. Indeed, by construction [see Eqs. (2)] we see that the intersection of the diagonal in quadrants II and IV with the patterns are the locus of points such as $(t_{i+1}-t_i) = (t_{i+3}-t_{i+2})$ and therefore defines an order-one orbit as two successive times define a period.

The general aspect of the first-order variability diagram constructed from T_i is the same as in the preceding case (see Fig. 7). However, as expected, the individual subpatterns show a different structure. A magnification of events around the origin is depicted in Fig. 7 and again we see marked dissymmetries between events in the four quadrants. As expected, we see a more complex relationship than the one shown in the first-order variability diagrams constructed from t_i.

In the present case the diagrams become blurred at fourth order as T_i is much longer than t_i. Here the number of points defining a curve decrease rapidly in parallel with the increase in the value of the coordinates.

Referring to the definition of T_i, we see that presently the first-order orbits of the Lorenz attractor are found by taking all points in the vicinity of the origin. The first-return map

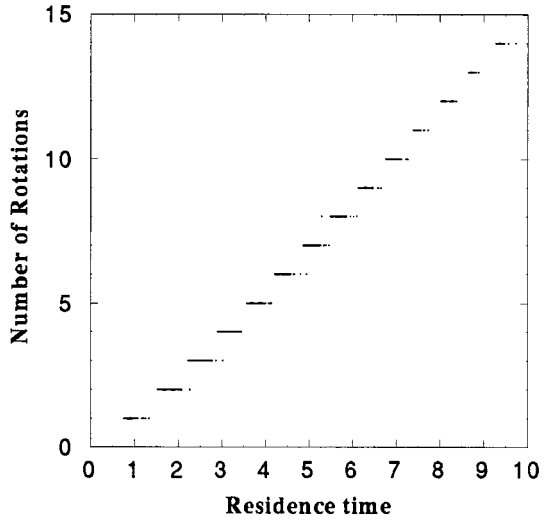

FIG. 6. Number of rotations as a function of residence time for the Lorenz attractor. All variables and parameters are dimensionless.

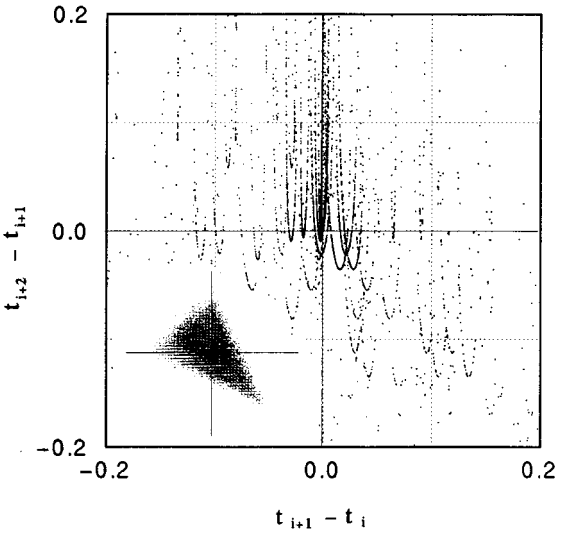

FIG. 7. First-order variability diagram for T_i and the details of events around the origin. All variables and parameters are dimensionless.

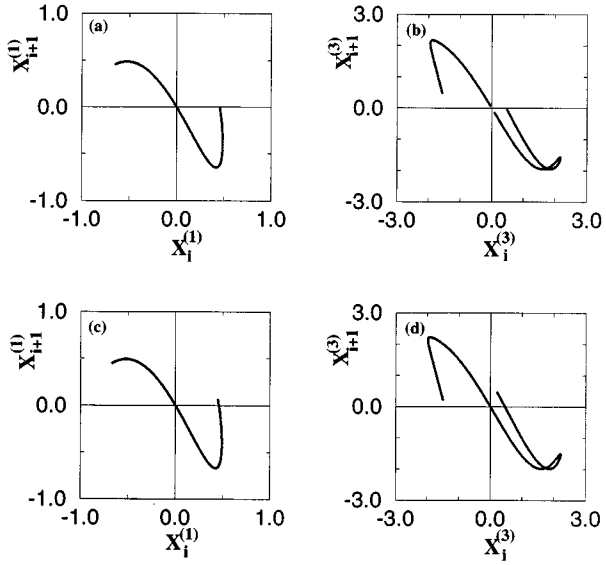

FIG. 8. (a) and (b) First- and third-order variability diagrams constructed from the logistic map for $\mu=0.919$. (c) and (d) Same as (a) and (b), but for $\mu=0.925$. $X_i^{(1)}, X_i^{(3)}$ are defined by Eqs. (1) with $r_i=x_i$. All variables and parameters are dimensionless.

from these points will give the periods of the first-order orbits. The second-order orbits are found by examining the intersections of the patterns in quadrants II and IV with the diagonal.

Higher-order variability diagrams are a rapid and convenient means for assessing the degree of stability of the orbits of first-order. Indeed, the cluster of points in the nth-order variability diagram and in the vicinity of (0,0) defines the complex relationships between $n+2$ consecutive intervals. However, $n+2$ equal intervals are also a possibility. Their occurrence may be seen from the first-return maps and will determine orbits of first order. As the order of the diagrams increases gradually the longer periods disappear. It seems that the shortest period is the most stable one. The value of n for which an existing orbit disappears is a measure of its stability. This example shows that it is possible to obtain additional information about the extensively studied Lorenz attractor with a simple graphical tool.

V. LOGISTIC MAP

In order to demonstrate the sensitivity of the method for detecting changes in system dynamics with a minimum amount of labor, we analyze the time series generated by the well-known logistic map defined by the equation

$$x_{k+1}=4\mu x_k(1-x_k), \quad \mu\in(0,1], \quad x_k\in[0,1]. \qquad (5)$$

Whenever μ increases to the accumulation point $\mu_\infty=0.892\,48...$, the time series generated by Eq. (5) starts to be chaotic. As μ continues to increase from μ_∞, the state of the system undergoes a period-doubling bifurcation of the chaotic bands until $\mu=\mu_{c1}=0.919\,64\ldots$; then the system enters into the fully developed chaotic regime.

Figures 8(a) and 8(b) show the first- and third-order variability diagrams for the logistic map with $\mu=0.919$. One sees from the first-order variability diagram that in this attractor only large-small-large and small-large-small sequences of x values are possible. We increase gradually the value of μ to 0.925 with a step $\Delta\mu=0.000\,01$ in order to follow changes in system dynamics. The corresponding first- and third-order variability diagram, for example, for $\mu=0.925$ [see Figs. 8(c) and 8(d)], show new combinations of events in the first quadrant not seen for lower values of μ. This change starts from $\mu=\mu_{c1}=0.919\,64\ldots$. This indicates a deceleration of dynamics over three consecutive values. Therefore, we conclude that the two attractors represent different dynamics. The change in dynamics is more apparent in the third-order diagram of Figs. 8(b) and 8(d). We note the absence of the sequence of five consecutive points in the attractor computed with $\mu=0.925$ around the origin of the coordinate system. This rules out the presence of consecutive and equal x.

For $\mu=0.920$, the probability to find a point in the first-order variability diagram, which populates quadrants I, II, III, and IV are 1.12%, 49.44%, 0%, and 49.44%, respectively and for $\mu=0.925$ they are 4.84%, 47.58%, 0%, and 47.58%, respectively. The zero probability of points in quadrant III means that there do not exist three consecutive decreasing values of x for any value of μ. In Fig. 9 we quantified the percentages of the number of threesomes in each quadrant for values of μ starting from 0.90 to $\mu=1$ with a step $\Delta\mu=0.001$. We see from Fig. 9 that only quadrants II and IV are populated until the value $\mu=0.919\,64\ldots$ is reached, whereby the population of threesomes starts to appear in quadrant I. It is interesting to note that for all values of μ, the populations in quadrants II and IV are always the same and there is no population in quadrant III. The peaks or ravines in the curves correspond to the periodic windows in the bifurcation diagram. For example, the plateau around $\mu\approx0.96$ stems from a period-three window. Ignoring the influence of the windows, the percentage in quadrant I has a tendency to increase with μ, whereas in quadrants II and IV the percentages decrease.

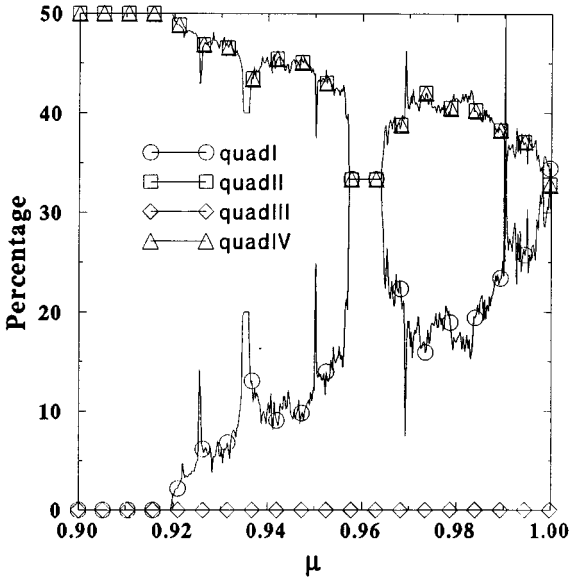

FIG. 9. Percentages of the number of points in the four quadrants of the first-order variability diagram obtained from the logistic map as a function of the parameter μ. Curves marked with ○, □, ◇, and △ represent the percentages in quadrants I, II, III, and IV, respectively.

The logistic map has been studied extensively in the literature from different points of view [30]. For example, in the framework of a general theoretical approach [31], one introduces a density function that is an eigenfunction of a probability-preserving kernel. Thus one computes eigenvalues and eigenfunctions of the dynamical system.

In the example treated here, we have limited ourselves to the region of fully developed chaos. The information gathered from our diagrams about the structure of the attractor is very different from the previous studies and is complementary to the previous works. We relate three, four, five, etc., consecutive events in the time series. Events of different magnitude may produce identical points in a two-dimensional diagram. We have shown that this method is extremely sensitive as a very small change in the value of μ gives rise to a qualitatively different diagram obtained with inexpensive computation. Therefore, we see that the method of variability diagrams is a fast and efficient tool for rapid and visual inspection of some aspects of the dynamics of the logistic map in the chaotic regime.

VI. CONCLUSION

We have introduced here a simple graphical method that projects the trajectories of chaotic attractors into various planes in such a way as to unveil very subtle correlations between consecutive sequences of events. The merit of the method resides in the fact that these sequences may extend over more than ten events. The sequences with similar relationships but not the same absolute values may appear as well-defined structures in a two-dimensional diagram. The advantage of this mapping is that, although the sequences may take into account more than three consecutive events, the two-dimensional projections are extremely helpful visual aides for elucidation of some aspects of chaotic dynamics. Moreover, the algorithm is very simple and computationally inexpensive. We showed the advantages of the method for a detailed study of an abnormal electrocardiogram, which would not have been possible either with the standard techniques prevailing in the medical literature such as standard deviation of RR intervals or with fast Fourier transforms of the same quantities. The usual nonlinear techniques estimating the invariants of motion will not be of much use for understanding the detailed nature of the joint heart-pacemaker dynamics. With our method we show that the pacemaker tries to keep the heart in a reasonable pace, for RR intervals ranging from 520 to 600 msec. However, eventually the arrythmia of the sick heart takes over for short episodes. We can even quantify the amount of time the pacemaker lost control over the sick heart and determine the extent of the arrythmia.

In the case of Lorenz-attractor we showed that the succession of residence times around the two fixed points obeys well-defined rules, which is not surprising as we are in the presence of deterministic chaos. Moreover, we showed that the unstable orbits of first order could be found easily by a visual inspection of the second-order diagrams. Another interesting feature of our diagrams is that with simple graphical views we determine the number of rotations around the two fixed points and their successions.

In the case of the well-known and extensively studied logistic map, we showed that a slight change in the parameter μ, which determines the route to chaos, can change the nature of the attractor considerably. We have seen that a very small increase in μ at $\mu=\mu_{c1}$ introduces a combination of sequences in the dynamics not seen for lower values of μ. Again we cannot think of a method that can make such a distinction so easily by such a simple manner. Therefore, we believe that the variability diagrams are a fast, easy, visual, and inexpensive tool for the study of some aspects of the chaotic attractors. The analysis does not require stationarity of the data set as the relative values over short sequences are plotted. Noise will generate a background cloud from which deterministic structures will emerge if present. Our method is especially useful for complex experimental time series such as biological data.

ACKNOWLEDGMENTS

We are especially grateful to Professor H. Ector from the Catholic University of Leuven for furnishing us with the unusual ECG recordings. We are indebted to N. Ellis and C. Lourenco for fruitful discussions. This work was supported by the Commission of the European Communities within the framework of the EC-RUSSIA collaboration, in accordance with ESPRIT Contract No. P9282-ACTCS.

[1] A. Babloyantz, in *Quantitative Measures of Dynamical Complexity in Nonlinear System*, edited by N. Abraham *et al.* (Plenum, New York, 1989).
[2] M. S. Casdagli, J. D. Eubank, D. Farmer, and J. Gibson, Physica D **51**, 52 (1991).
[3] J. Theiler Phys. Rev. A **41**, 3038 (1990).
[4] D. Ruelle, Proc. R. Soc. London, Ser. A **427**, 241 (1990).
[5] P. Grassberger, T. Schreiber, and C. Schaffrath, Int. J. Bifurcation Chaos **1**, 521 (1991).
[6] A. Babloyantz, Electroencephaloigr. Clin. Neurophysiol. **78**, 402 (1991).
[7] S. Sato, M. Sano, and Y. Sawada, Prog. Theor. Phys. **77**, 1 (1987).
[8] P. S. Landa and M. G. Rosenblum, Physica D **48**, 232 (1991).
[9] W. Liebert, K. Pawelzik, and H. G. Schuster, Europhys. Lett. **14**, 521 (1991).
[10] E. J. Kostelich and J. A. Yorke, Phys. Rev. A **38**, 1649 (1988).
[11] C. Grebogi, E. Ott, and J. A. Yorke, Phys. Rev. A **37**, 1711 (1988).
[12] J. P. Eckmann, Oliffson, S. Komphorst, D. Ruelle, and S. Ciciberto, Phys. Rev. A **34**, 4971 (1986).
[13] D. Broomhead and G. P. King, Physica D **20**, 217 (1986).
[14] P. Grassberger and I. Procaccia, Physica D **9**, 189 (1983).
[15] R. Badii, E. Brun, M. Finardi, L. Flepp, R. Holzner, J. Parisi, C. Reyl, and J. Simonet, Rev. Mod. Phys. **66**, 1389 (1994).
[16] CHAOS **2**, (1) (1992) chaos focus issue on periodic orbit theory, edited by P. Cuitanovic.
[17] D. Gallez and A. Babloyantz, Phys. Lett. A **161**, 247 (1971).
[18] J. Guckenheimer and Ph. Holmes, *Nonlinear Oscillations, Dynamical Systems and Bifurcations of Vectors Fields* (Springer-Verlag, Berlin, 1983).
[19] R. Artuso, E. Avrell, and P. Cvitanovic, Nonlinearity **3**, 325 (1990).
[20] P. Cvitanovic, Phys. Rev. Lett. **61**, 2729 (1988).
[21] A. Babloyantz and P. Maurer, Phys. Lett. A **221**, 43 (1996).
[22] A. Babloyantz and P. Maurer, in *EUROSPACE '95, Proceedings of the Seventh International Conference, Istanbul, Turkey, 1995* (Monduzzi Editore SpA, Bologna, Italy, 1995).
[23] R. E. Kleiger, J. P. Miller, J. T. Bigger, and A. J. Moss, Am. J. Cardiol. **59**, 256 (1987).
[24] A. Babloyantz and A. Destexhe, Biol. Cybern. **58**, 203 (1988).
[25] S. Akselrod, D. Gordon, F. A. Ubel, D. C. Shannon, A. C. Barger, and R. J. Cohen, Science **213**, 220 (1981).
[26] M. A. Woo, W. G. Stevenson, D. Moser, R. B. Trelease, and R. M. Harper, Am. Heart J. **123**, 704 (1992).
[27] *Handbook of Mathematical Functions*, edited by M. Abramowitz and A. Stegun (Dover, New York, 1965), p. 877.
[28] J. J. Zebrowki, W. Poplawska, and R. Baranowski, Phys. Rev. E **50**, 4187 (1994).
[29] V. Balakrishnan, G. Nicolis, and C. Nicolis, J. Stat. Phys. **86**, 199 (1997).
[30] R.L. Devaney, *An Introduction to Chaotic Dynamic Systems* (Addison-Wesley, Reading, MA, 1987).
[31] S.-J. Chang and J. Wright, Phys. Rev. A **23**, 1419 (1981).